On the Absolute Calibration of IUE High Resolution Spectra

I. INTRODUCTION

The absolute calibration of IUE low resolution spectra is obtained, as described by Bohlin et al. (1980), by comparing uncalibrated IUE low resolution spectra with spectra of a selected set of standard stars observed by OAO-2 and TD-1 (S2/68).

In this paper we intend to show that a reliable absolute calibration can also be achieved for IUE high resolution spectra. The method followed here is based on the comparison, at the different wavelengths, of IUE high resolution spectra with uncalibrated low resolution spectra of the same target. In order to prove that the obtained calibration is independent of the kind of target used, an heterogeneous sample of representative spectra was analyzed including some of the IUE calibration standards as well as cooler stars, peculiar stars and emission line objects for which both high and low resolution suitable spectra obtained through the IUE large entrance aperture were available.

II. METHOD

Let us indicate with n_λ, the slit-integrated net Flux Number per time unit (sec) extracted from an IUE low resolution spectrum of a given target obtained through the large aperture. The corresponding absolute flux will be:

$$F_\lambda = n_\lambda \, S_\lambda^{-1} \qquad \text{erg cm}^{-2} \text{ s}^{-1} \text{ Å}^{-1} \tag{1}$$

where S_λ^{-1} is the inverse sensitivity for IUE low resolution spectra (Bohlin et al. 1980). If we indicate with N_λ the slit integrated net Flux Number per time unit extracted from a high resolution large aperture spectrum of the same target, then the corresponding energy distribution can be written as:

$$F_\lambda = N_\lambda \left(\frac{n_\lambda}{N_\lambda}\right) S_\lambda^{-1} = N_\lambda C_\lambda S_\lambda^{-1} \text{ erg cm}^{-2} \text{ s}^{-1} \text{ A}^{-1} \tag{2}$$

where the ratio:

$$C_\lambda \equiv n_\lambda / N_\lambda \tag{3}$$

can be determined empirically from a sample of targets for which both high and low resolution spectra are available. The product $C_\lambda S_\lambda^{-1}$ will naturally represent the inverse sensitivity of high resolution spectra.

C_λ can be easily determined from pairs of low-high resolution spectra by measuring the average values of n_λ and N_λ in correspondence to a selected number of spectral windows if possible free of strong spectral features. This method was followed in our first approach to the problem.

A more precise procedure - here followed - consists in convolving high resolution spectra with the point spread function corresponding to low resolution spectra. After the original resolution has been degraded, the spectrum is directly compared point by point, with the corresponding low resolution spectrum. In particular, if $\lambda_i (i=1,2,...N)$ are the sampled wavelengths in the low resolution spectrum, the convolved high resolution spectrum can be computed as:

$$N_{\lambda_i} = \frac{\sum_{K=K_1}^{K_2} N_{\lambda_K} (\lambda_K - \lambda_{K-1}) \exp\left[-4 \ln(2) (\lambda_K - \lambda_i)^2/FWHM\right]}{\sum_{K=K_1}^{K_2} (\lambda_K - \lambda_{K-1}) \exp\left[-4 \ln(2) (\lambda_K - \lambda_i)^2/FWHM\right]} \quad (4)$$

where K_1 and K_2 are suitable integration limits over the profile and FWHM is the full width at half maximum of the low resolution point spread function, assumed to be a gaussian. Since FWHM is a slow function of wavelength for both SWP and LWR low resolution spectra, it has been assumed to be a constant in our calculations and namely 6 and 9 Å for SWP and LWR low resolution spectra respectively.

The overlapping parts of the high resolution orders were eliminated using a suitable computer subroutine. Since for wavelengths larger than about 1930 Å in the SWP camera there is no overlap between successive orders, the convolution above was truncated in the appropriate range of wavelengths eventually not covered. This problem does not exist for the LWR camera since the high resolution orders do overlap up to the long wavelength end of the camera.

III. THE CALIBRATION SAMPLE

The high resolution calibration is based on the analysis of a representative sample of heterogeneous sources for which both high and low resolution IUE spectra were available. Spectra obtained through the small IUE entrance aperture were not considered since the small aperture transmission depends on the observing conditions and cannot be determined with enough accuracy. However, preliminary results obtained by Ake and Holm (1980), indicate that the ratio between large and small aperture spectra of the same star is grey within ± 3% for high resolution spectra. Therefore relative energy distributions can also be obtained from small aperture high resolution spectra.

The calibration sample includes some of the hot standard stars (BD+28° 4211 and HD 60753) already used for the low resolution absolute calibration (Bohlin et al. 1980) as well as cooler stars and emission line sources. Detailed information on the images used is reported in Table 1a (continuous sources) and Table 1b (emission line sources). Only spectra with suitable exposure times were included in the sample. Over-exposed spectral regions, eventually present in a few spectra, were not considered for the computation of the average C_λ . For some of the targets spectra with different exposure levels were considered in order to detect any dependence of C_λ on the data quality. All spectra were processed at VILSPA using the standard image processing system (SIPS).

IV. INTERORDER BACKGROUND

It is well known that the separation between the orders of IUE high resolution spectra rapidly decreases with order number (i.e. with decreasing wavelength) while the width of the orders is only linearily decreasing with the order number. As a consequence, at sufficiently short wavelengths, the flux levels half-way between the orders, where IUE SIPS extracts the background, will be increased by the wings of the adjacent orders. However, the actual contamination of a given order by light from the adjacent orders will be small. Hence, the extracted background at these short wavelengths for both the LWR and the SWP cameras will be artificially enhanced and the net IUE fluxes will be underestimated. This effect will be naturally large, in these wavelength ranges, for spectra of continuous sources while it will be negligible for emission line sources with faint or no continuum detectable at high resolution.

The way the smaller separation of the orders at the short wave ends of the cameras artificially enhances the interorder background for continuous sources is shown in Fig. 1 representing a typical scan of the SWP camera in a direction almost perpendicular to the orders. It is interesting to give a rough evaluation of the magnitude of the effect on the extracted net spectra. To this purpose, let us indicate with R_λ the ratio between the true net spectrum N°_λ (i.e. derived using the true camera background) and the net spectrum N_λ currently derived using IUESIPS:

$$R_\lambda = N^\circ_\lambda / N_\lambda \qquad (5)$$

where N_λ and N°_λ are both measured at the central wavelength λ of each order. It can easily be shown that, to a first approximation, R_λ is only a function of the distance, D, between two adjacent orders m and m-1 and of the full width at half maximum W of the orders perpendicular to the dispersion direction and not of the kind of object observed. Namely,

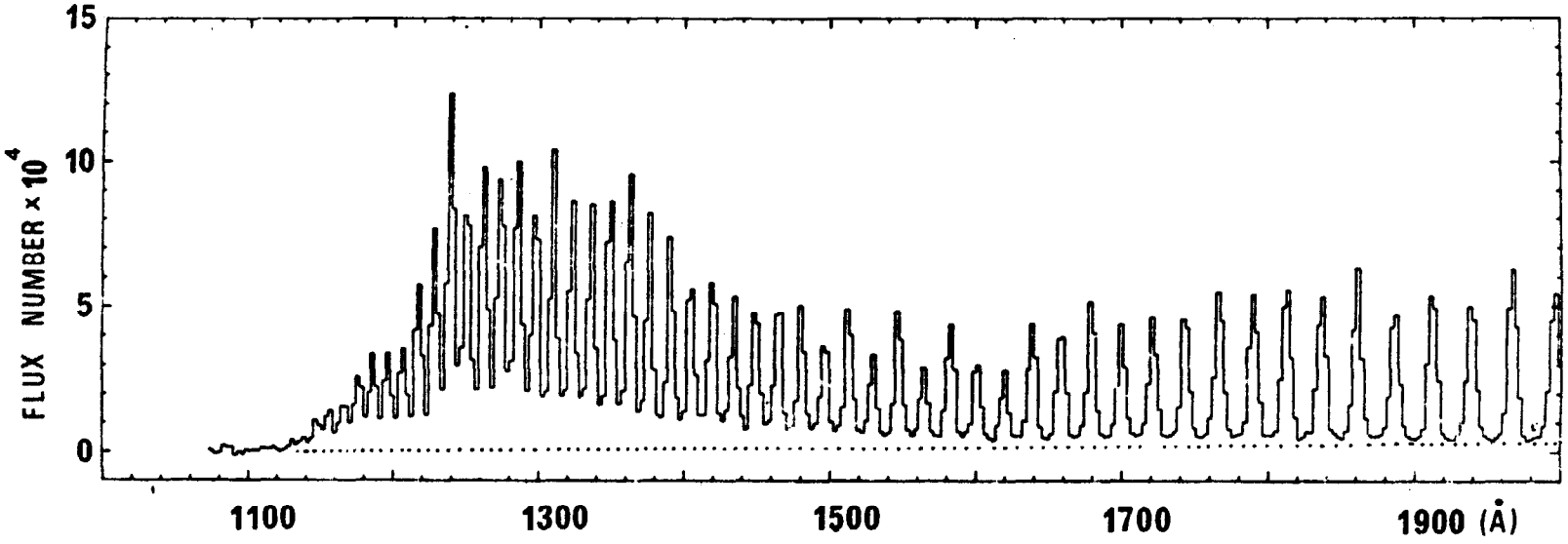

FIGURE 1: Typical cross cut of a high resolution SWP spectrum of a continuous source in a direction perpendicular to the orders passing through the center of the camera. Ordinates give the Gross spectrum in Flux Numbers. The dotted line represents our guess of the true camera background

we have:

$$R_\lambda \simeq [1-2\exp(-(\frac{D}{W})^2 \ln 2)]^{-2} \quad (6)$$

where the wavelength dependence of the right hand term is contained in D and W since $\lambda = K/m$ Å (K=137725 for the SWP camera and K=231150 for the LWR camera). In order to determine the behaviour of R_λ, the dependence of D and W on the order number was derived by a least squares fitting of cross scans of the kind shown in Fig. 1 with a sum of gaussian lines following the method described by Cassatella (1976). A linear background level as indicated by the dotted line in Fig. 1, representing our guess of the true camera background, was adopted in the fitting. The values of D and W so obtained are plotted in Fig. 2a,b as a function of the order number, together with the corresponding value of R_λ. As it appears from the figure, the orders width is almost constant with wavelength. Using the SIPS interorder background level instead of the linear background here adopted would lead to larger values of the order's width at the short wavelength ends of the cameras as shown by Bianchi (1980) and Schiffer (1980). It also appears from the figure that at the short wavelength ends of the cameras the net fluxes extracted from high resolution continuous spectra are currently underestimated up to roughly 60%.

Different considerations apply to the case of emission line objects with faint or no continuum detectable at high resolution. In this case the interorder background is close to the camera background and then R_λ is expected to be close to unity at every wavelength. In particular, the results in Fig. 2 indicate that the absolute calibration for emission line sources will deviate from that of continuous sources in the wavelength ranges where R_λ is larger than unity (high interorder background regions), i.e. for $\lambda \leqslant 1500$ Å in the SWP camera and $\lambda \leqslant 2400$ Å in the LWR camera. Longward of these wavelengths the calibration for either class of objects is expected to be the same.

V. RESULTS AND DISCUSSION

The C_λ function was computed for spectra of continuous sources and for emission line objects using the calibration sample in Table 1. The computations were performed separately for the two classes of objects both for the reasons explained in §IV (the C_λ curve is expected to be different at the short wavelength ends of the cameras for the two classes of objects) and for methodological reasons. Actually, due to the faint continuum observed in the high resolution spectra of emission line objects, only the emission lines can be reliably used to derive C_λ, therefore a manual measurement of the line fluxes was preferred instead of applying the convolution in eq. (4).

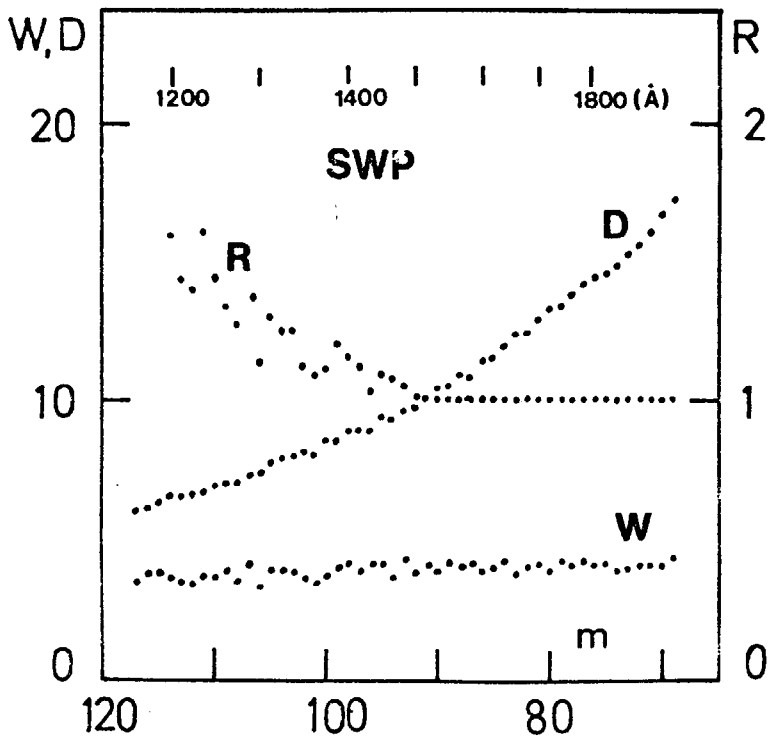

FIGURE 2a:

Behaviour of D (distance in pixels between two successive orders) and W (full width at half maximum, in pixels, of the order m measured perpendicular to the dispersion direction) as a function of the order number m for the SWP camera. Also plotted is the function R from equation 6.

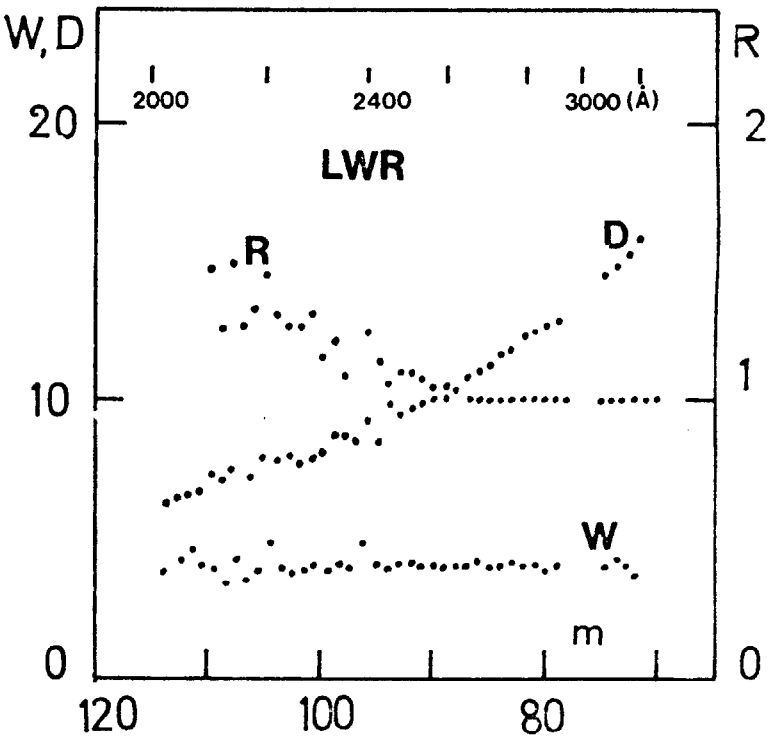

FIGURE 2b:

Same as Figure 2a for the LWR camera.

a) Continuous sources

The derived values of C_λ for continuous sources computed in 25 Å bins and averaged over the sample of images in Table 1a is reported in Fig. 3 for the SWP camera and Fig. 4 for the LWR camera together with the corresponding rms deviations of the individual values of C_λ for each bin. The adopted smoothed curve through the data is reported for convenience both in Figs. 3 and 4, and in Table 2.

The rms error on C_λ is typically of 4-5% or better for $\lambda \geq 1400$ Å in the SWP camera and $\lambda \geq 2400$ Å in the LWR camera and up to 7-8% shortwards of these wavelengths. The errors found are reasonably close to the reproducibility limits ($2\sigma \simeq 6\%$) of IUE low resolution spectra (Bohlin et al. 1980, Cassatella et al. 1980), so confirming the validity of the calibration here derived. The larger errors found at the short wavelength ends of the cameras can essentially be ascribed to the lower sensitivity of the cameras in these wavelength regions and to uncertainties in the inter-order background in the region where the order overlap is large.

An independent determination of the C_λ curve, based on two spectra for each camera of ζ Sco and η UMa, provided by Ake and Holm (1980) confirms the results in Table 2.

A few representative examples of application of the high resolution calibration here derived are shown in Figs. 5 and 6 where small spectral intervals of the calibrated and convolved spectra of R Cr B, BD+28° 4211, HD 60573, and HD 102567 are compared with the corresponding low resolution spectra. It appears from these figures that the point to point fluctuations between the pairs of high-low resolution spectra are generally better than 10%, occasionally reaching larger values at a few points. Anyhow, the validity of the calibration is confirmed by the good precision obtained on the integrated fluxes. This is clear from the above figures where, in each spectral window, the percentage deviation of the convolved and calibrated high resolution spectra with respect to the calibrated low resolution spectra is reported.

The C_λ curve for continuous sources is quite accurate even at the short wavelength end of the cameras. This is shown in Fig. 7 where the high resolution SWP convolved spectrum of BD+75° 325 is compared, after calibration, with the corresponding low resolution spectrum.

b) Emission line sources

For emission line objects, an independent calibration was derived using the images listed in Table 1b.

In some of the low resolution spectra the continuum was quite strong. Therefore, in order to measure the line fluxes it was first necessary to estimate the location of the stellar continuum. The values of C_λ so derived are plotted in the same Figs. 3 and 4 in order to be compared with the C_λ curve for continuous spectra. Different symbols are used according to the quality of the measurements.

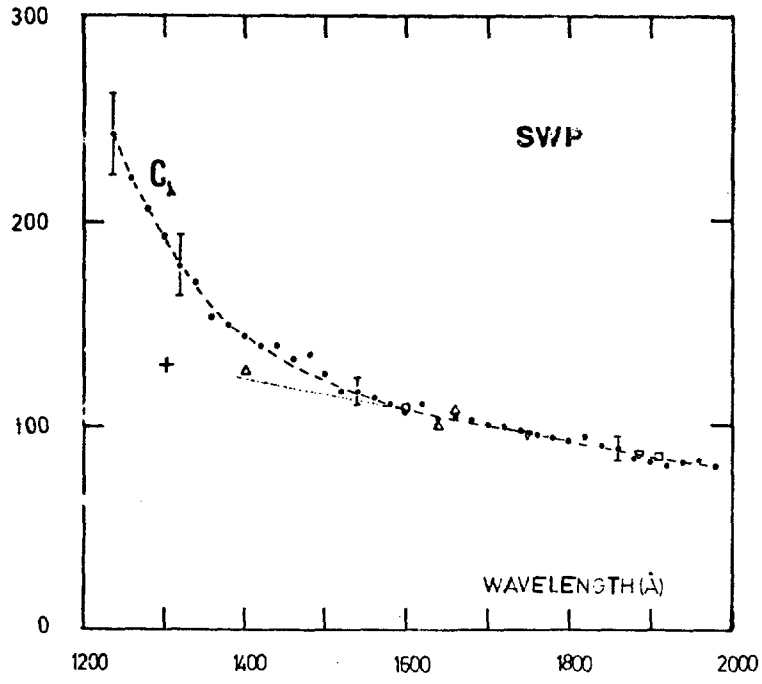

FIGURE 3: C_λ curve for the SWP camera obtained for: a) Continuous sources (dots and dashed line). b) Emission line spectra with faint or no continuum; the data are labelled according to their quality (+ uncertain; ○, □, △, ▽ : reliable values obtained, respectively from 1, 2, 3, or 4 pairs of spectra. Error bars are indicated at a few wavelengths.

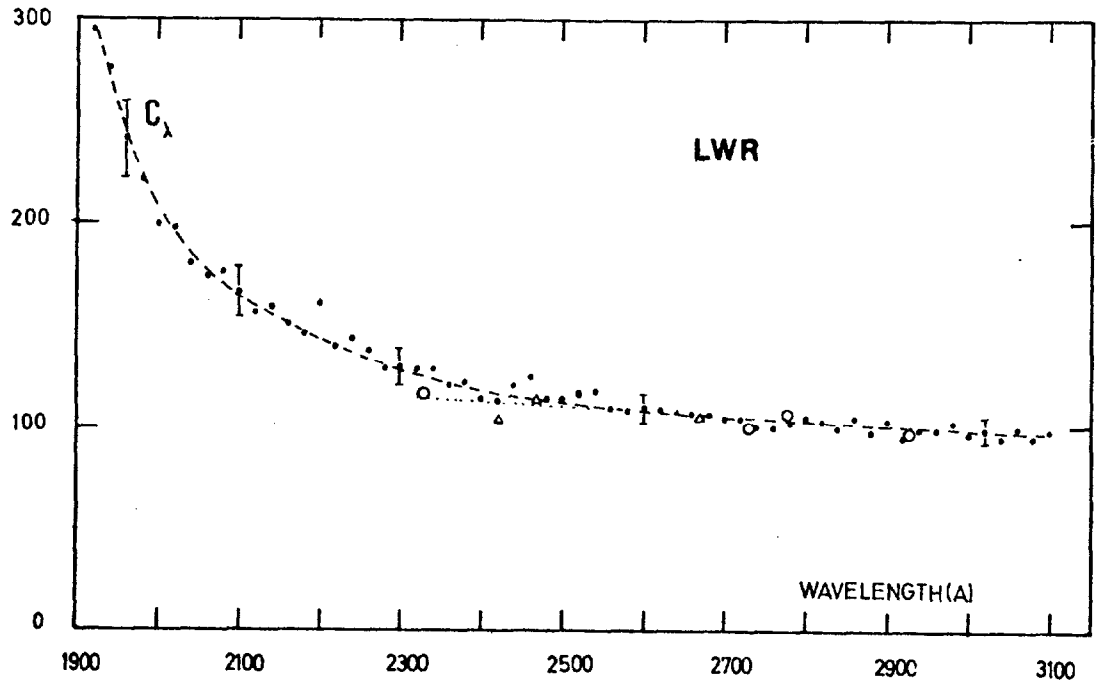

FIGURE 4: C_λ curve for the LWR camera. Symbols as for Figure 3.

No good quality data were available for $\lambda \leq 1400$ Å in the SWP spectra and $\lambda \leq 2300$ Å in the LWR spectra. Therefore the high resolution calibration of emission line spectra was restricted to the following wavelength intervals: 1400-1975 Å (SWP camera) and 2300-3100 Å (LWR camera). In these intervals the C_λ curve can be fitted to a straight line:

$$C_\lambda = 228.009 - 0.0755\lambda \quad 1400 \leq \lambda \leq 1975 \text{ Å} \tag{7}$$

$$C_\lambda = 167.099 - 0.0229\lambda \quad 2300 \leq \lambda \leq 3100 \text{ Å} \tag{8}$$

The above relations also fit very well the $C\lambda$ curve for continuous spectra longward of 1575 Å for the SWP camera and 2500 Å for the LWR camera, in approximative agreement with the estimated wavelength limits given in §IV.

The accuracy of eqs. (7) and (8) is about 4-5% longward of 1600 Å in the SWP camera and 2400 Å in the LWR camera, but is less precise shortward of these wavelengths because they are based on less and more uncertain data than for continuous spectra.

Eqs. (7) and (8) were applied to calibrate spectra of the emission line stars V1016 Cyg and RR Tel. Some examples are provided in Fig. 8 from which it appears that a good match is obtained between the calibrated high resolution convolved spectra and the corresponding low resolution spectra.

It is important to note that the present high resolution calibration was derived using the current production Intensity Transfer Functions (ITF) for the SWP and LWR cameras. The LWR ITF is the one that was implemented with EXTLOW as described in Bohlin et al. (1980). The SWP ITF is the corrected version documented in Holm (1979). Recently, Holm (1980) has reported about the magnitude of the non linearity in the LWR ITF. According to the preliminary tests, it appears that assigned fluxes may be too high by 10% to 15% for pixels having Flux Numbers less than 4800. Holm (1981) also finds additional non linearity in the SWP ITF such that fluxes assigned to pixels having Flux Numbers less than 2000 may be too low by as much as 20%. The effects of these non linearities on the high resolution calibration cannot yet be evaluated. Therefore, we advise users that substantial errors may result if our calibration is applied to underexposed spectra.

VI. CONCLUSIONS

It has been shown that a reliable absolute calibration can be obtained for high resolution IUE spectra of point sources obtained through the large entrance slit. The accuracy of the calibration table for continuous sources is typically of the order of 4-5% for $\lambda \geq 1400$ Å in the SWP camera and $\lambda \geq 2400$ Å in the LWR camera and is slightly worse at shorter wavelengths.

For emission line objects with faint or no continuum the calibration only covers a part of the observed spectral range and it is represented by eqs. (7) and (8). The extension to the short wavelength end of the cameras, where the calibration is expected to be different from that of continuous sources, was prevented by the lack of good quality data in these spectral regions.

VII. ACKNOWLEDGEMENTS

We are grateful to Drs. P. Gondhalekar, K. Northover and M. Penston for their useful comments. We also acknowledge the valuable contributions and suggestions by Dr. A. Holm.

REFERENCES

Ake, B., Holm, A.: 1980, Report to the 3 Agency Meeting

Bianchi, L.: 1980, private communication

Bohlin, R.C., Holm, A.V., Savage, B.D., Snijders, M.A.J., Sparks, V.M.: 1980, Astron. Astrophys. 85, 1

Cassatella, A.: 1976, Astron. Astrophys. 48, 281

Holm, A.V.: 1979, NASA IUE Newsletter N° 7, p. 27

Holm, A.V.: 1981, private communication

Holm, A.V.: 1980, Report to the 3 Agency Meeting

Schiffer, F.H., III: 1980, Report to the 3 Agency Meeting

A. Cassatella
D. Ponz
P.L. Selvelli

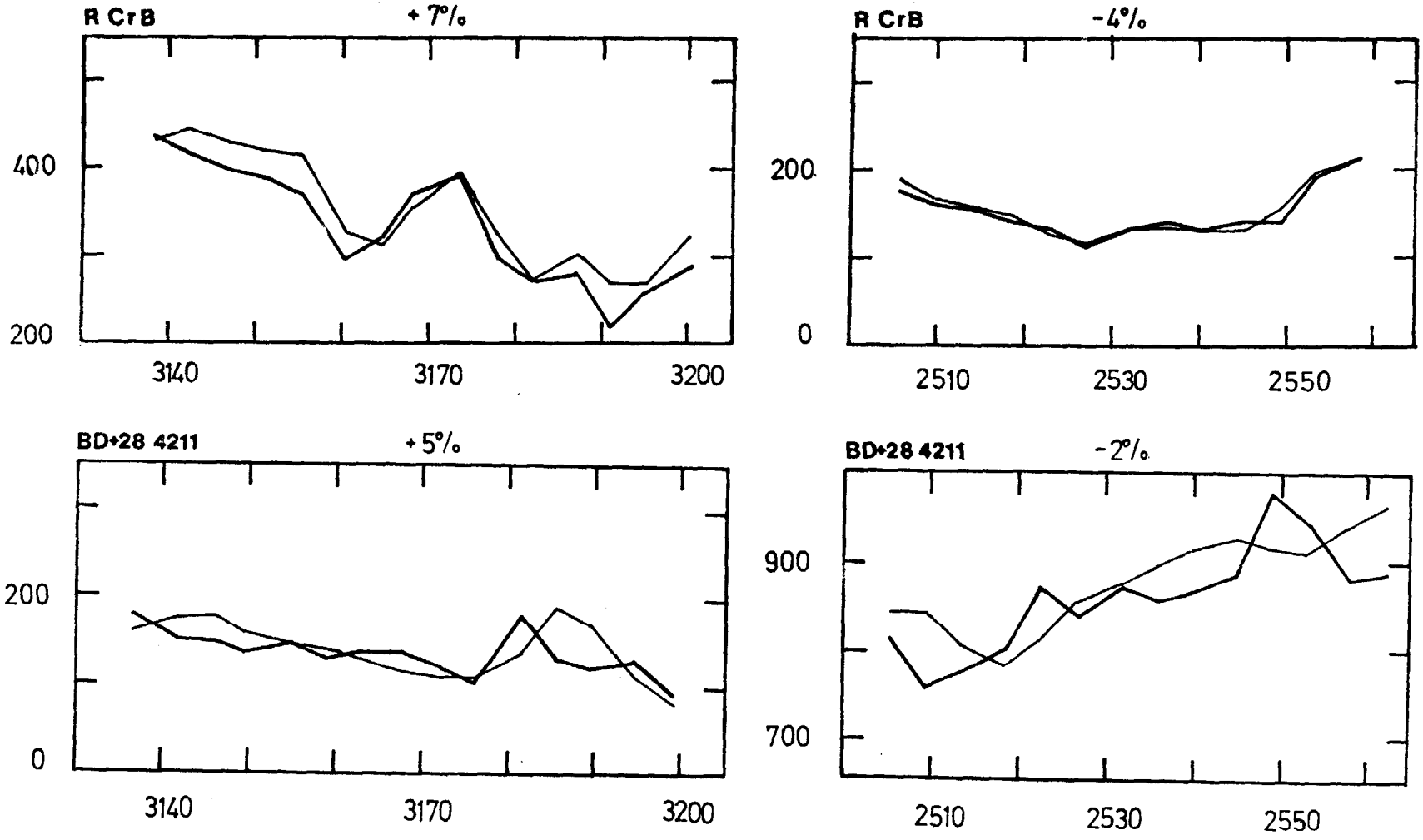

FIGURE 5: Comparison between low resolution LWR spectra of continuous sources with convolved high resolution spectra after the calibration curve in Fig. 4 is applied. Ordinates are in FN/sec. The percentage mean deviation of the total flux (high minus low resolution) in each window is indicated in the figure. Thin line: high resolution convolved and calibrated spectrum; thick line: low resolution spectrum.

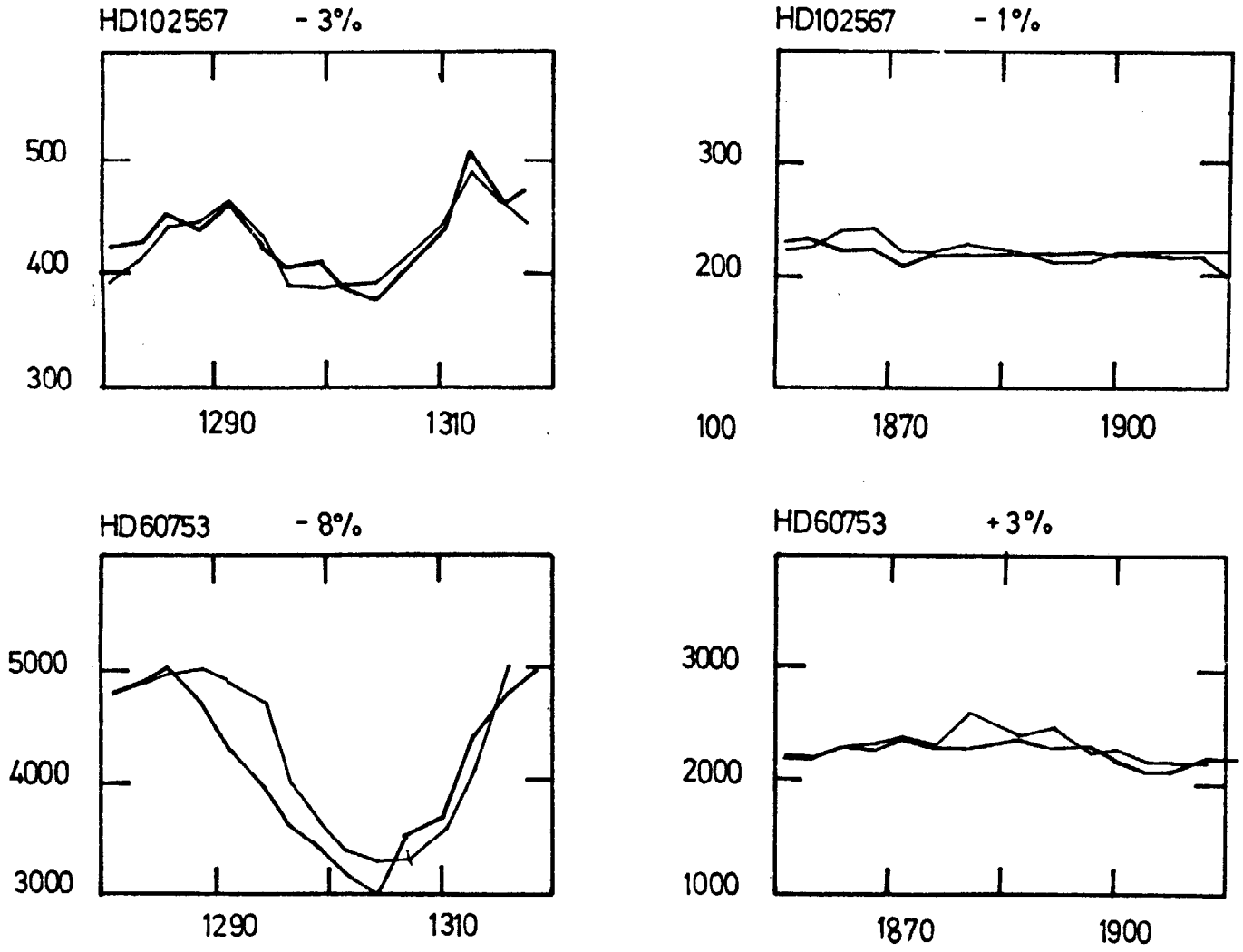

FIGURE 6: Comparison of low resolution SWP sepctra of continuous sources with convolved high resolution spectra after the correction curve in Fig. 3 is applied. Symbols are as in Fig. 5.

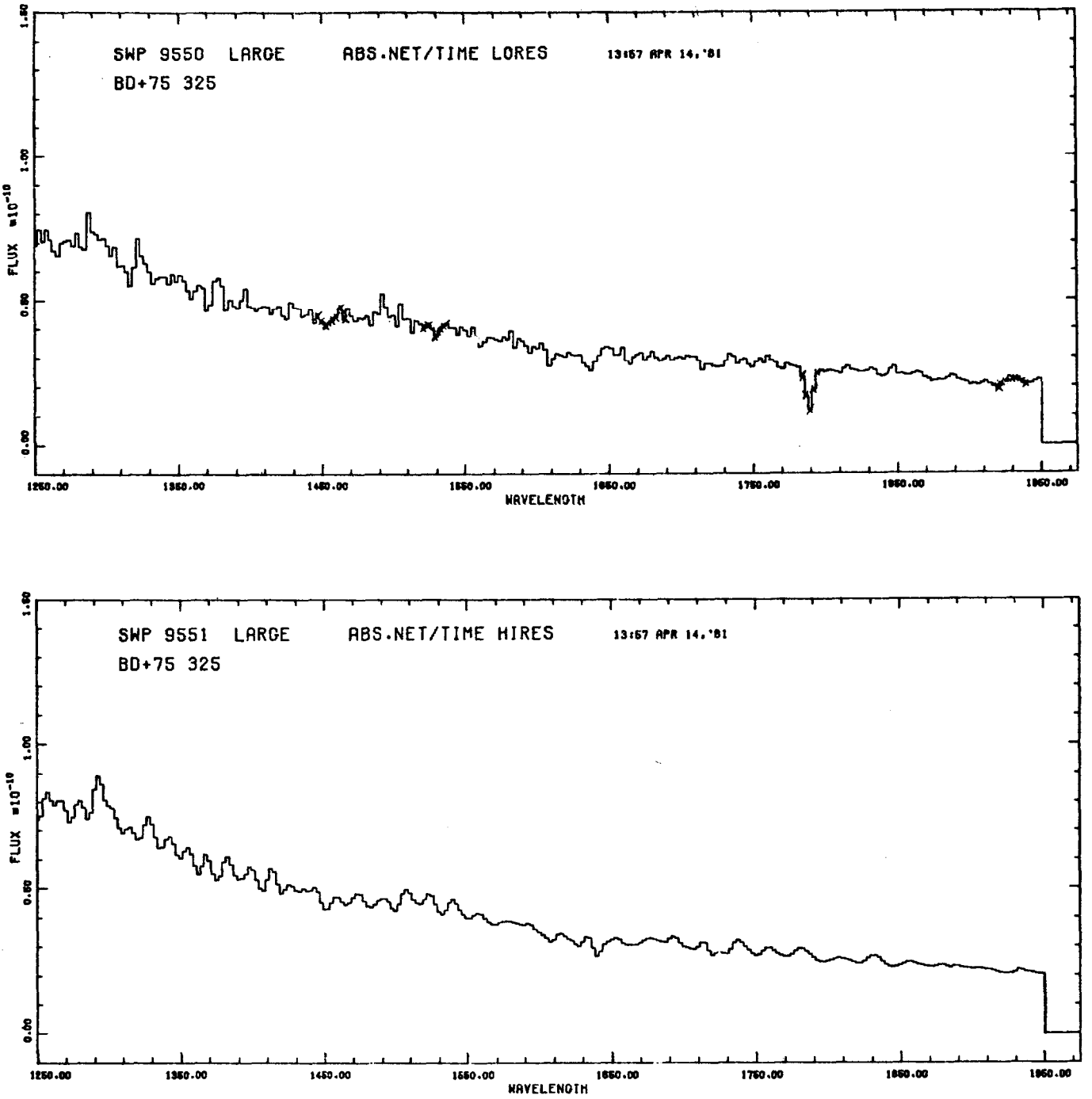

FIGURE 7: Comparison between the energy distribution of BD+75°325 as derived from a low dispersion spectrum (top) and a high resolution convolved and calibrated spectrum (bottom). It is possible to see that a good accuracy is obtained except for a small ripple effect.

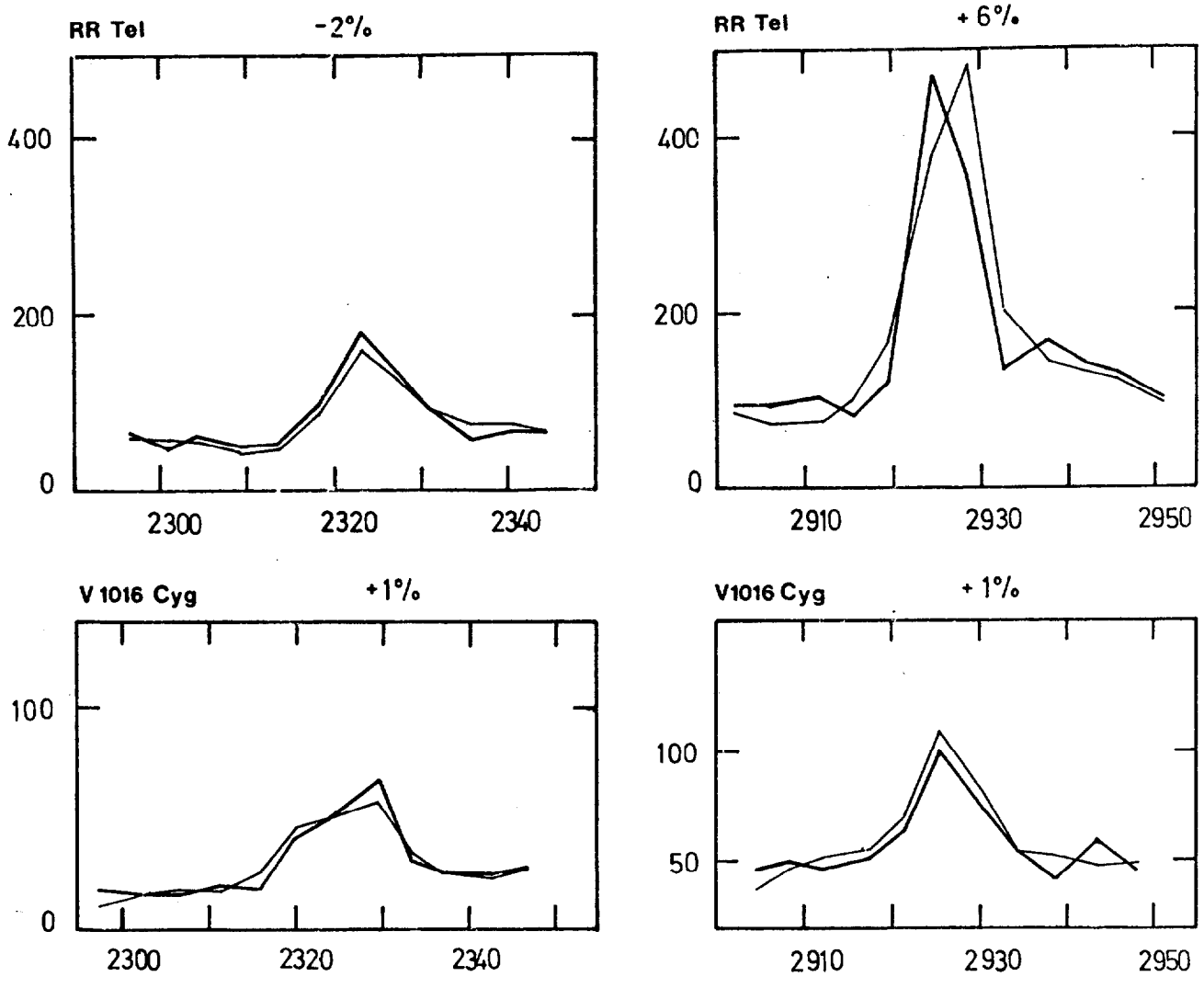

FIGURE 8: Comparison of low resolution LWR spectra of emission line sources with convolved high resolution spectra after the correction curve in Fig. 4 is applied. Symbols are as in Fig. 5.

TABLE 1 - a) CONTINUOUS SPECTRA

TARGET	IMAGE	RESOLUTION	DURATION (sec)	DATE	QUALITY* C	E
BD+28°4211 (sdO)	SWP 7292	LO	30	7 DEC 79	5	0
	SWP 5778	HI	2400			
	SWP 7428	LO	30	18 DEC 79	5	0
	SWP 5779	HI	3600			
HD 187473 (Ap)	SWP 8279	LO	60	17 MAR 80	5	0
	SWP 8280	HI	3840	17 MAR 80	5	0
HD 125248 (Ap)	SWP 8282	LO	25	17 MAR 80	5	0
	SWP 8281	HI	2100	17 MAR 80	7	0
HD 269546 (B3I)	SWP 8042	LO	300	25 FEB 80	3	4
	SWP 8043	HI	14040	25 FEB 80	4	4
HD 60753 (B3IV)	SWP 8703	LO	10	8 APR 80	5	0
	SWP 8704	HI	780	8 APR 80	5	0
	SWP 8703	LO	10	8 APR 80	5	0
	SWP 8705	HI	960	8 APR 80	5	0
HD 102567 (B1Ve)	SWP 8585	LO	150	29 MAR 80	6	0
	SWP 8586	HI	3000	29 MAR 80	5	0
HD 24534 (O9.5Ve)	SWP 8587	LO	14	29 MAR 80	5	0
	SWP 8588	HI	1200	19 MAR 80	5	0
HD 269546	LWR 7005	LO	180	25 FEB 80	6	0
	LWR 7004	HI	9000	25 FEB 80	4	0
BD+28°4211 (sdO)	LWR 6815	LO	100	29 JAN 80	6	0
	LWR 5024	HI	4800	12 JUL 79	5	0
	LWR 6816	LO	80	29 JAN 80	5	0
	LWR 5024	HI	4800	12 JUL 79	5	0
	LWR 6284	LO	60	2 DEC 79	5	0
	LWR 5471	HI	3600	27 AUG 79	4	0
HD 60753 (B3IV)	LWR 7449	LO	7	8 APR 80	5	0
	LWR 7450	HI	720	8 APR 80	5	0
HD 190229 (B8II-III)	LWR 8104	LO	6	22 JUN 80	5	0
	LWR 8103	HI	570	22 JUN 80	6	0
HD 190429 (Oe)	LWR 8106	LO	11	23 JUN 80	5	0
	LWR 8105	HI	1050	22 JUN 80	5	0

TABLE 1 - b) EMISSION LINE SPECTRA

TARGET	IMAGE	RESOLUTION	DURATION (sec)	DATE	QUALITY* C	QUALITY* E
RR Tel	SWP 8607	LO	75	31 MAR 80	2	6
(symbiotic)	SWP 9606	HI	300	31 MAR 80	1	6
	SWP 8606	LO	90	31 MAR 80	2	6
	SWP 8609	HI	600	31 MAR 80	1	6
	SWP 7355	LO	180	31 MAR 80	2	6
	SWP 7356	HI	800	31 MAR 80	1	6
	SWP 8911	LO	35	4 MAY 80	2	6
	SWP 9812	HI	600	4 MAY 80	2	6
	SWP 8606	LO	90	31 MAR 80	2	6
	SWP 8608	HI	300	31 MAR 80	1	6
	SWP 8607	LO	75	31 MAR 80	2	6
	SWP 8609	HI	600	31 MAR 80	2	6
	SWP 10553	LO	30	5 NOV 80	2	5
	SWP 10554	HI	1200	5 NOV 80	2	6
	LWR 7662	LO	150	4 MAY 80	2	6
	LWR 7663	HI	1380	4 MAY 80	2	6
	LWR 9239	LO	180	5 NOV 80	3	6
	LWR 9238	HI	1800	5 NOV 80	2	6
V1016 Cyg	SWP 5611	LO	1200	24 JUN 79	5	9
(symbiotic)	SWP 5613	HI	3600	24 JUN 79	0	7
	SWP 5611	LO	1200	24 JUN 79	5	9
	SWP 5612	HI	1200	24 JUN 79	0	5
	LWR 6225	LO	300	25 NOV 79	3	7
	LWR 6229	HI	9720	25 NOV 79	3	7
	LWR 6226	LO	100	15 NOV 79	3	7
	LWR 6228	HI	3240	15 NOV 79	2	6
	SWR 6227	LO	900	25 NOV 79	5	8
	LWR 6229	HI	9720	25 NOV 79	3	7
CI Cyg	SWP 9255	LO	2400	10 JUN 80	2	6
(symbiotic)	SWP 9256	HI	10800	10 JUN 80	1	6
Z And	SWP 9940	LO	3600	28 AUG 80	4	6
(symbiotic)	SWP 9939	HI	2400	28 AUG 80	1	5

* The Quality factor is a measure of the exposure level of the spectrum in both the continuum (C) and the emission lines (E). It ranges from Ø (no exposure) to 9 (completely saturated). A well exposed spectrum will have a quality factor of about 5.

TABLE 2

a) SWP CAMERA

WAVELENGTH (A)	C_λ
1250	230
1275	208
1300	193
1325	176
1350	163
1375	152
1400	143
1425	136
1450	131
1475	126
1500	122
1525	118
1550	114
1575	110
1600	108
1625	105
1650	103
1675	101
1700	100
1725	98
1750	96
1775	94
1800	92
1825	90
1850	88
1875	86
1900	84
1925	82
1950	81
1975	80

b) LWR CAMERA

WAVELENGTH (A)	C_λ
1925	292
1950	259
1975	229
2000	207
2025	191
2050	180
2075	171
2100	165
2125	159
2150	153
2175	149
2200	143
2225	139
2250	136
2275	132
2300	129
2325	126
2350	122
2375	120
2400	118
2425	116
2450	115
2475	114
2500	113
2525	112
2550	110
2575	109
2600	108
2625	107
2650	106
2675	105
2700	104.5
2725	104.0
2750	103.5
2775	103.0
2800	102.5
2825	102.0
2850	101.5
2875	100.5
2900	100.2
2925	100.0
2950	99.5
2975	99.0
3000	98.5
3025	98.0
3050	97.5
3075	97.0
3100	96.5